Dy3+ doped GaGeSbSe fiber long-wave infrared emission

F. Starecki, G. Louvet, J. Ari, A. Braud, Jean-Louis Doualan, R. Chahal, I. Hafienne, C. Boussard-Pledel, Virginie Nazabal, P. Camy

Dy^{3+} doped GaGeSbSe fiber long-wave infrared emission

F. Starecki[a*], G. Louvet[b,c], J. Ari[b,c], A. Braud[a], J-L. Doualan[a], R. Chahal[b], I. Hafienne[a], C. Boussard-Plédel[b], V. Nazabal[b] and P. Camy[a]

[a] Laboratoire CIMAP UMR 6252 CEA-CNRS-ENSICaen, Université de Caen, 14050 Caen, France

[b] Institut des Sciences Chimiques de Rennes, (ISCR), UMR-CNRS 6226, Université de Rennes 1, France.

[c] COPL, Université Laval, Québec, Canada

ABSTRACT

We report on the mid-wave infrared (MWIR) and long-wave infrared (LWIR) emissions of a 1000 ppm Dy^{3+} doped $Ga_5Ge_{20}Sb_{10}Se_{65}$ chalcogenide fiber. Following a short-wave infrared (SWIR) optical pumping at 0.92, 1.12 and 1.32 µm using commercial laser diodes, LWIR luminescence around 7.3 µm ($^6H_{7/2} \rightarrow {}^6H_{9/2}$ transition) was recorded for the first time to the best of our knowledge along with MWIR emissions around 4.3 µm and 5.4 µm with a Dy^{3+} doped $Ga_5Ge_{20}Sb_{10}Se_{65}$ fiber. Frequency dependent spectroscopic investigation clearly shows that this LWIR luminescence originates from the $^6H_{7/2}$ manifold. Spectroscopic properties of this Dy^{3+} doped material and the comparison with its equivalent sulfide Dy^{3+}:$Ga_5Ge_{20}Sb_{10}S_{65}$ glass are presented.

Keywords: Chalcogenide glasses, rare earth, infrared, optical fiber

*florent.starecki@ensicaen.fr; phone +33231452566

1. INTRODUCTION

For infrared (IR) photonic applications, chalcogenide glasses properties offer a wide range of possibilities thanks to the combination of a transparency window in the LWIR (8-12 µm) spectral domain, consequence of its typical low phonon energy, and thermomechanical properties still allowing a convenient use with standard preparation techniques, e.g. fiber drawing or polishing steps [1, 2]. These glasses proved efficient for sensing applications like molecule fingerprint detection using fiber evanescent wave spectroscopy for instance [3]. Taking advantage of the molding properties of these glasses, 3D chalcogenide glass printing was recently demonstrated [4], enabling the fabrication of complex optical components. Also, these materials are compatible with deposition techniques such as magnetron sputtering, permitting the realization of rare earth (RE) doped infrared optical waveguides with single-mode optical propagation at 4.7 µm [5]. The strong non-linear refractive index of these chalcogenide glasses also permits the development of original mid-infrared supercontinuum source emitting up to 13 µm [6].

Also, these glasses can be efficiently doped with trivalent rare earth ions [7] making possible the development of fibered infrared fluorescence sources [8, 9] while the development of RE-doped fibered laser sources in the MWIR is an ongoing attractive research field [10]. The $Ga_5Ge_{20}Sb_{10}Se_{65}$ glass host has a low band-gap energy, and its transparency domain spans from 1 to 11 µm. The average phonon energy is about 250 cm^{-1} [11], indicating a potential embedded RE emission up to 8 µm. This type of LWIR emissions was demonstrated for both Tb^{3+} [12] and Sm^{3+} doped $Ga_5Ge_{20}Sb_{10}Se_{65}$ glasses [13], respectively emitting around 8.0 µm and 7.3 µm. Embedded in such a glass host, Dy^{3+} ions could also provide potentially a 7.3 µm emission ($^6H_{7/2} \rightarrow {}^6H_{9/2}$ transition). Dy^{3+} is also known for generating two MWIR (4.3 and 5.4 µm) emissions. As a matter of fact, a 4.3 µm laser operation has already be obtained in a Dy^{3+} doped $PbGa_2S_4$ crystal, using a powerful 1.7 µm pump laser diodes [14] now available. In glass fibers, laser operation at 2.8 µm was reported in Dy^{3+}doped InF_3 fiber [15].

The 4.3 µm fluorescence of a Dy^{3+} doped $Ga_5Ge_{20}Sb_{10}S_{65}$ fiber was already used for the development of a mid-IR carbon dioxide sensor based on CO_2 absorption measurement at 4.3 µm [16]. A second type of CO_2 sensor was recently developed using this 4.3 µm source to probe the gas concentration variation, but additionally implementing a MWIR-NWIR wavelength converter to create an all-optical CO_2 detection [17].

This sulfide glass was chosen for its ability to generate an efficient 4.3 µm luminescence following a 920 nm pumping, thanks to its low phonon energy (350 cm^{-1}) and large transparency window. But reducing the phonon energy can allow closely spaced upper manifolds to initiate radiative emissions, which can be the case in a selenide glass host. In this work, we present the MWIR and LWIR emissions from 1000 ppm Dy^{3+} doped $Ga_5Ge_{20}Sb_{10}Se_{65}$ chalcogenide fibers under 1.3 µm and 1.12 µm optical pumping. In particular, we present, for the first time to our knowledge, emissions from the $^6H_{7/2}$ level at 1.1 µm and 7.3 µm in Dy^{3+} doped selenide fibers. The spectroscopic characterization of the low-lying manifolds involved in these transitions is presented and compared to the Dy^{3+} properties in the sulfide $Ga_5Ge_{20}Sb_{10}S_{65}$ glass.

2. MATERIAL AND METHODS

The glasses were elaborated from high purity raw materials, and melted in sealed ampoules in a rocking furnace. The melt was water-quenched and annealed below T_g for some hours to decrease the glass internal stress. A more extensive glass preparation is detailed in [18]. Following this process, 1000 ppm Dy^{3+} doped $Ga_5Ge_{20}Sb_{10}Se_{65}$ and Dy^{3+}:$Ga_5Ge_{20}Sb_{10}S_{65}$ glass rods were elaborated, from which 350 µm diameter single core fibers were drawn. The selenide preform has been developed using $TeCl_4$ and MgO to specifically limit the presence of Ge-O bonds because it plays a very important role in the efficiency of emissions in the LWIR spectral range.. Also, the Dy^{3+}:$Ga_5Ge_{20}Sb_{10}S(Se)_{65}$ glass structure analysis was performed through K-edge of Ge, Ga, S and L_{III}-edge of Dy EXAFS for sulfide glasses and by Raman scattering spectroscopic for both composition [18]. Absorption spectra were recorded using a Perkin-Elmer Lambda 1050 spectrophotometer. The emission experiments were carried out using three different laser diodes with optical power of few watts at the wavelengths of 0.92, 1.12 and 1.32 µm, coupled to standard 105/125 µm silica fibers. The chalcogenide fibers were mounted in FC/PC connectors and their end faces were polished. The IR signal at the fiber output was collimated using a C037TME-F lens (Thorlabs), and appropriate long-pass filters (Spectrogon) were used to remove any parasitic higher order contribution from the transmitted pump or SWIR Dy^{3+} luminescence. Adapted diffraction gratings were also used for each wavelength domain. For the fiber experiments, an incident power of 700 mW from the 1.3 µm laser diode (Q-Photonics QSM-1320-4.5) was used, while for LWIR fluorescence experiments a 1.12 µm laser diode (Innolume LD-1120-BA-6W) was used as pumping source (incident power of 1.6 W). Fluorescence spectra were corrected from the setup spectral response using a black-body-like source (Arcoptix MIR-2000-9000). Lifetimes experiments were performed on bulk samples using a Continuum Horizon OPO as pulsed laser source. SWIR luminescence was recorded using a thermoelectrically cooled InGaAs detector, while MWIR and LWIR spectra were recorded using a liquid-nitrogen cooled HgCdTe detector.

3. RESULTS AND DISCUSSION

3.1 Fiber attenuation

In Figure 1 is reported the fiber attenuation comparison between the Dy^{3+}-doped $Ga_5Ge_{20}Sb_{10}Se_{65}$and it counterpart sulfide glass. Figure 1 also features the main impurities absorption bands, like S-H (4.0 µm) or Se-H (4.5 µm).

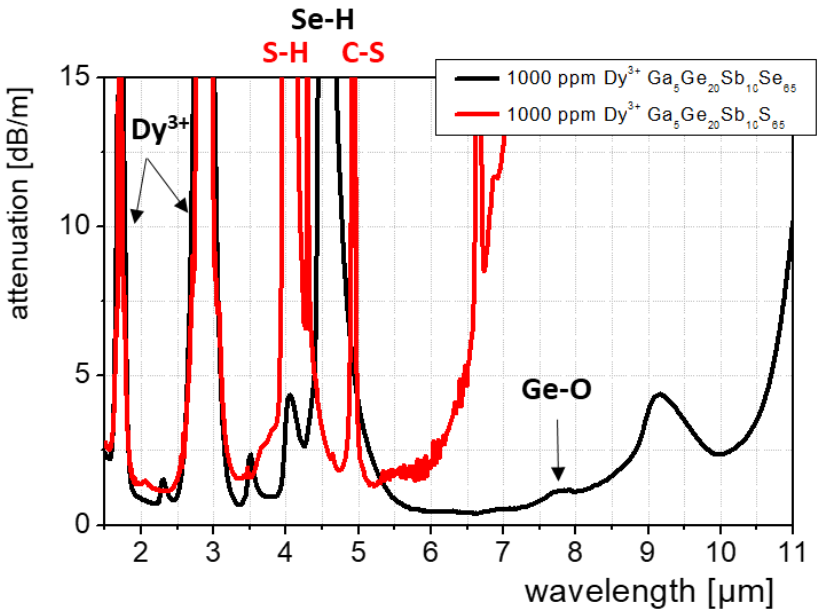

Figure 1: comparison of sulfide and selenide Dy^{3+} doped $Ga_5Ge_{20}Sb_{10}(S \text{ or } Se)_{65}$ fiber attenuation spectra.

The purification process using $TeCl_4$ and MgO is assumed to lead to a significant reduction in the amount of Ge-O bonds within the selenide glass [Figure 1], which absorption peak is at 7.7 µm. The background losses at this wavelength is 1.2 dB/m, which is a key issue for efficient LWIR luminescence generation and propagation since it is resonant with the Dy^{3+} $^6H_{7/2} \rightarrow {}^6H_{9/2}$ emission. Figure 1 shows that the sulfide fiber multiphonon edge lies at 7 µm, restricting the use of this material to MWIR applications.

3.2 Absorption properties and Judd-Ofelt analysis

The spectroscopic study of Dy^{3+}:$Ga_5Ge_{20}Sb_{10}Se_{65}$ is presented here and compared to the Dy^{3+}:$Ga_5Ge_{20}Sb_{10}S_{65}$ sulfide glass properties. The spectroscopic study for this Dy^{3+} doped sulfide glass was already reported [19]. For the Dy^{3+} :$Ga_5Ge_{20}Sb_{10}Se_{65}$ material, only a brief description of the emission properties could be found in [18], and thus we present here a comprehensive study of Dy^{3+}:$Ga_5Ge_{20}Sb_{10}Se_{65}$ including Judd-Ofelt calculations and fluorescence lifetimes measurements. In Figure 2(a) is reported the absorption cross-sections of the Dy^{3+} ion embedded in $Ga_5Ge_{20}Sb_{10}S_{65}$ and $Ga_5Ge_{20}Sb_{10}Se_{65}$ glass hosts, while Figure 2(b) shows the expected Dy^{3+} emissions in the sulfide and selenide matrices.

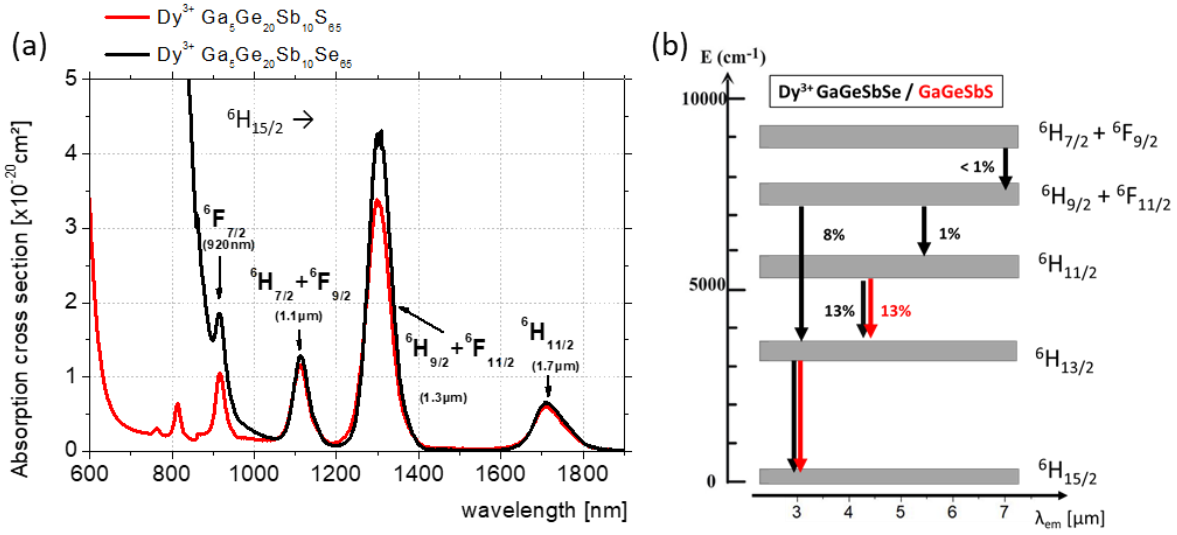

Figure 2: comparison of: (a) absorption cross-sections and (b) MWIR and LWIR expected emissions for the Dy^{3+}: $Ga_5Ge_{20}Sb_{10}S_{65}$ and Dy^{3+}: $Ga_5Ge_{20}Sb_{10}Se_{65}$ glasses.

Figure 2(a) indicates that Dy^{3+} absorption cross-sections are comparable from a sulfide to a selenide matrix. One can notice on one hand a difference for the $^6H_{9/2}$ + $^6F_{11/2}$ absorption band, with a peak value of $4.2x10^{-20}$ cm^2 in the selenide material. On the other hand, 1.1 µm ($^6H_{7/2}$ + $^6F_{9/2}$) and 1.3 µm ($^6H_{11/2}$) absorption cross-sections are similar between the sulfide and selenide material. The $^6F_{7/2}$ absorption band is at the edge of the selenide material transparency window, so that a significant power fraction will be directly converted into heat when pumping Dy^{3+} ions at 920 nm. Therefore, a special care must be taken when pumping at this wavelength so as to avoid optical damage on the fiber. Another possibility is to excite the Dy^{3+}:$Ga_5Ge_{20}Sb_{10}Se_{65}$ glass at longer wavelength than 920 nm to generate MWIR or LWIR emissions. The only available pumping band for LWIR luminescence generation from the $^6H_{7/2}$ level is a direct excitation of this very same level at 1.1 µm. For the MWIR luminescence at 5.4 µm ($^6H_{9/2}$ + $^6F_{11/2}$ → $^6H_{11/2}$ transition) and at 4.3µm ($^6H_{11/2}$ → $^6H_{13/2}$transition) the direct pumping of the $^6H_{9/2}$ level at 1.3µm is more efficient since the absorption cross-section is larger at 1.3µm than at 1.1µm.

Some MWIR and all LWIR transitions are dominated by non-radiative relaxations within a sulfide glass host because of its larger phonon energy than in a selenide material [18]. The multiphonon relaxation rates for sulfide glasses, given in [20], indicates that the $^6H_{7/2}$ and $^6H_{9/2}$ manifolds luminescence is quenched so that the MWIR emissions are limited to the $^6H_{11/2}$ → $^6H_{13/2}$ transition at 4.3 µm and $^6H_{13/2}$ → $^6H_{15/2}$ transition at 2.8 µm. For the Dy^{3+}-doped selenide material, the lower phonon energy reduces the multiphonon relaxation rates for both $^6H_{7/2}$ and $^6H_{9/2}$ manifolds (for the sake of clarity the mention of the combined $^6F_{9/2}$ and $^6F_{11/2}$ levels will be implicit in the rest of the text). These two latter manifolds can thus potentially give rise to MWIR to LWIR emissions when considering the $^6H_{7/2}$ - $^6H_{9/2}$ and $^6H_{9/2}$ - $^6H_{11/2}$ energy gaps [Figure 2(b)].

From the Dy^{3+}:$Ga_5Ge_{20}Sb_{10}Se_{65}$ cross-section calibrated absorption spectrum, the Judd-Ofelt (JO) parameters were calculated to have an assessment of the radiative lifetimes and branching ratios. A standard fitting procedure was used to derive the $\Omega_{2,4,6}$ parameters which reproduce the integrated absorption band values while taking into account magnetic dipole contributions [21]. The four $^6H_{7/2;\ 9/2;}$

$_{11/2;\ 13/2}$ integrated absorption bands were considered as input data for this JO analysis. The $^6F_{7/2}$ absorption band was not considered since it lies at the edge of the bandgap [Figure 2(a)]. The corresponding Judd-Ofelt $\Omega_{2,4,6}$ parameters are (9.6; 2.9; 2.4) ($\times 10^{-20}$ cm^2). The radiative lifetimes and branching ratios were then calculated with this set of $\Omega_{2,4,6}$ parameters and are reported in Table 1.

Table 1. Dy^{3+} $Ga_5Ge_{20}Sb_{10}Se_{65}$ transition average wavelength, radiative lifetimes and branching ratios (β) derived from the Judd-Ofelt analysis.

Manifolds		λ_{av} [µm]	τ_{rad}(JO) [ms]	β
From	To			
$^6H_{7/2} + {}^6F_{9/2}$	$^6H_{9/2} + {}^6F_{11/2}$	7.52	0.13	0.004
	$^6H_{11/2}$	3.18		0.03
	$^6H_{13/2}$	1.81		0.31
	$^6H_{15/2}$	1.11		0.65
$^6H_{9/2} + {}^6F_{11/2}$	$^6H_{11/2}$	5.51	0.11	0.01
	$^6H_{13/2}$	2.38		0.08
	$^6H_{15/2}$	1.30		0.91
$^6H_{11/2}$	$^6H_{13/2}$	4.21	1.63	0.13
	$^6H_{15/2}$	1.71		0.87
$^6H_{13/2}$	$^6H_{15/2}$	2.88	4.17	1.00

The radiative lifetimes and branching ratios presented in Table 1 should be compared to the same parameters derived for its sulfide counterpart Dy^{3+}:$Ga_5Ge_{20}Sb_{10}S_{65}$ [19]. The Dy^{3+} radiative lifetimes are found to be longer in the selenide matrix, except for the $^6H_{13/2}$ manifold, while branching ratios are quite comparable in the sulfide and selenide hosts. Considering now the MWIR and LWIR emission potentialities of the Dy^{3+}:$Ga_5Ge_{20}Sb_{10}Se_{65}$ fibers, it is worth noticing that the $^6H_{7/2} \rightarrow {}^6H_{9/2}$ (7.3 µm) has a poor branching ratio of 0.4%. However, Sm^{3+} doped $Ga_5Ge_{20}Sb_{10}Se_{65}$ glasses exhibit a clear LWIR emission around 7.4 µm with a similar branching ratio [13], so that one could expect to observe the Dy^{3+} emission at 7.3 µm.

The MWIR $^6H_{9/2} \rightarrow {}^6H_{11/2}$ transition around 5.4 µm has also a weak branching ratio of 1%, but this emitting level can be efficiently pumped directly owing to the strong $^6H_{15/2} \rightarrow {}^6H_{9/2}$ absorption (1.3 µm). The other Dy^{3+} MWIR emission is the 4.3 µm emission ($^6H_{11/2} \rightarrow {}^6H_{13/2}$), which is commonly observed in sulfide doped fiber and can be advantageously used for CO_2 detection for instance [19].

3.3 Lifetime measurements

Table 2 shows the fluorescence Dy^{3+} lifetimes measured in a 1000 ppm doped Dy^{3+}:$Ga_5Ge_{20}Sb_{10}Se_{65}$ glass, compared to the equivalent sulfide glass.

Table 2. 1000 ppm doped Dy^{3+} $Ga_5Ge_{20}Sb_{10}(Se_{65}$ or $S_{65})$ experimental fluorescence lifetimes.

manifold	Sulfide [18]	selenide
$^6H_{7/2}$	3 µs	42 µs
$^6H_{9/2}$	34 µs	230 µs
$^6H_{11/2}$	1.3 ms	1.46 ms
$^6H_{13/2}$	5.6 ms	3.3 ms

The fluorescence lifetimes of the Dy^{3+} $^6H_{7/2}$ and $^6H_{9/2}$ manifolds in the selenide glass are one order of magnitude longer than the ones in its sulfide glass counterpart. The $^6H_{7/2}$ and $^6H_{9/2}$ manifolds

fluorescence lifetimes goes from 3 to 42 µs and from 34 to 230 µs respectively. This lengthening of the lifetimes clearly illustrates the reduction of the phonon energy when going from a sulfur to a selenium based compound.

For the $^6H_{11/2}$ and $^6H_{13/2}$ manifolds, the measured fluorescence lifetimes are comparable in both hosts which can be expected since the $^6H_{11/2}$ to $^6H_{13/2}$ and $^6H_{13/2}$ to $^6H_{15/2}$ energy gaps are about 2350 and 3450 cm^{-1} respectively. These energy gaps are quite large compared to the 350 cm^{1} and 250 cm^{-1} of the sulfide and selenide host respectively meaning that the $^6H_{11/2}$ and $^6H_{13/2}$ are weakly affected by multiphonon relaxation processes.

3.4 MWIR luminescence

In this section, we will describe the luminescence properties of Dy^{3+}:$Ga_5Ge_{20}Sb_{10}Se_{65}$ fibers in the MWIR spectral domain. Figure 3(a) presents a comparison between a sulfide and selenide fiber with the same 120 mm length and the same 1000 ppm Dy^{3+} doping level. Following a 1.3 µm optical pumping with the same incident power of 700 mW. Figure 3(b) shows the 1.3 µm pumping and energy levels involved in this cascade luminescence process.

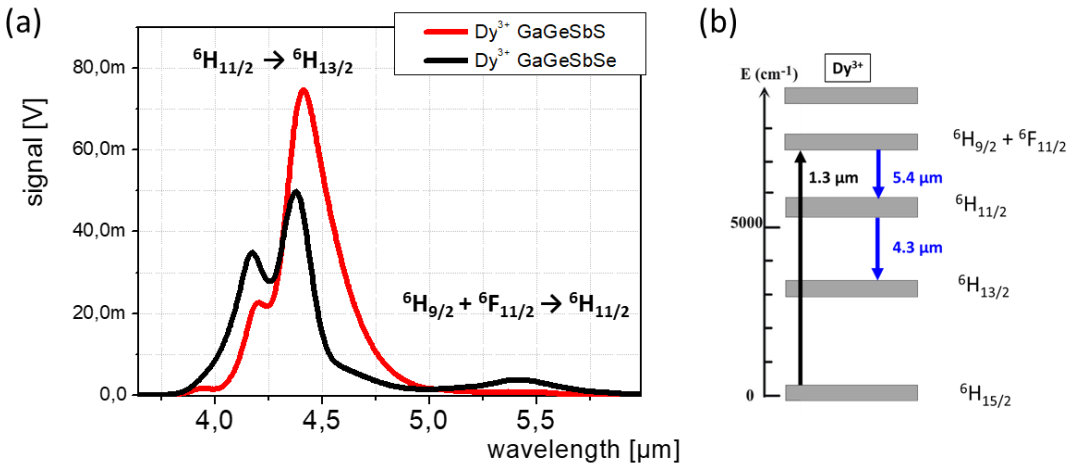

Figure 3: (a) 1000 ppm Dy^{3+}:$Ga_5Ge_{20}Sb_{10}Se_{65}$ and 1000 ppm Dy^{3} :$Ga_5Ge_{20}Sb_{10}S_{65}$ luminescence measurements for a 1320 nm pumping; (b) energy diagram and pumping scheme for the Dy^{3+} MWIR transitions.

The first noticeable MWIR emission band is the $^6H_{11/2} \rightarrow {}^6H_{13/2}$ transition around 4.3 µm). One can notice that the sulfide and selenide glass host do not exhibit the same emission line shape and this is most likely due to Se-H and S-H bonds absorption. As indicated in the fiber attenuation spectra [Figure 1], S-H and Se-H bonds absorption peaks are located at 4.0 and 4.5 µm, respectively. Therefore, the shorter wavelength part of the emission spectrum around 4µm in the sulfide glass is truncated by the S-H absorption while it is the longer wavelength part in the selenide host which is affected by the Se-H absorption. As a result, the Dy^{3+}-doped fiber luminescence central emission wavelength is shifted from 4.34 µm to 4.43 µm from the selenide to the sulfide glass host. Figure 3(a) features the $^6H_{9/2} \rightarrow {}^6H_{11/2}$ MWIR emission around 5.4 µm following the 1.3 µm pumping. This emission is recorded with a clear satisfactory signal to noise ratio in the selenide glass, whereas for the sulfide glass the emission intensity is one order of magnitude lower. Considering the shorter $^6H_{9/2}$

fluorescence lifetime of 34 µs in the sulfide host compared to the 230 µs recorded in the selenide glass, this low fluorescence intensity is to be expected.

Emission spectra are corrected from the setup spectral response, so that the 4.3 and 5.4 µm emission intensities can be compared in each glass. Because of its poor branching ratio (β=1%), the 5.4 µm ($^6H_{9/2} \rightarrow {}^6H_{11/2}$ transition) intensity is lower than the 4.3 µm ($^6H_{11/2} \rightarrow {}^6H_{13/2}$) (β = 13%). Additionally, as discussed earlier, the $^6H_{9/2}$ is more quenched by multiphonon relaxation than the $^6H_{11/2}$ level further reducing the intensity at 5.4 µm compared to 4.3 µm. Following the 1.3µm pumping, the Dy^{3+} excitation into the $^6H_{11/2}$ manifold is thus mostly due to this multiphonon relaxation from the $^6H_{9/2}$ level explaining why the 4.3 µm emission intensities are comparable in both glasses. Moreover, since the Dy^{3+} doping level and fiber lengths are identical in Figure 3, one can compare the 4.3 µm intensities from the two fibers. The sulfide fiber exhibits a higher intensity despite a slightly lower 1.3 µm absorption cross-section (Figure 2(a)). This illustrates the consequence of the 100 cm^{-1} shift of the glass host phonon energy from the selenide to the sulfide based chalcogenide glass leading to a higher multiphonon relaxation rate in the sulfide glass from the $^6H_{9/2}$ to the $^6H_{11/2}$ and thus to a larger $^6H_{11/2}$ population and subsequent 4.3 µm intensity. Under the same pumping conditions, a sulfide fiber is thus preferable to generate luminescence at 4.3 µm, while for an emission at 5.4 µm the Dy^{3+}-doped selenide material is more suitable.

3.5 LWIR luminescence

A practical way to assess the possibility to observe a LWIR luminescence is to record first the SWIR emission from the same emitting level, as illustrated in a previous LWIR study of Sm^{3+} doped selenide fibers [13]. In Dy^{3+} doped materials, the LWIR emission is expected to arise from the $^6H_{7/2}$ manifold. Consequently, the first step is to record the SWIR emission from this manifold around 1.15 µm ($^6H_{7/2} \rightarrow {}^6H_{15/2}$ transition). Figure 4 shows the $^6H_{7/2}$ and $^6H_{9/2}$ emissions recorded in the SWIR domain under optical pumping at 920 nm. A low pumping power (80 mW at 920 nm) was used to avoid optical damage on the fiber by the pump beam since the $^6H_{15/2} \rightarrow {}^6F_{7/2}$ absorption band lies on the edge of the band-gap (Figure 2(a)). The $^6H_{7/2} \rightarrow {}^6H_{15/2}$ transition has the highest branching ratio of the $^6H_{7/2}$ transitions (β=65%), creating favorable conditions to record this emission.

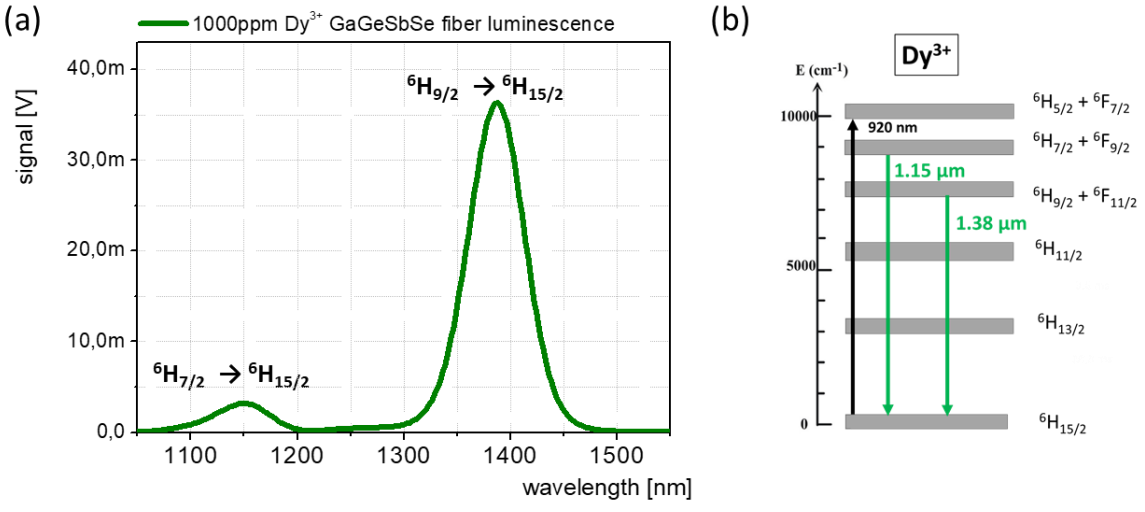

Figure 4: (a) SWIR luminescence of the 1000 ppm Dy^{3+} doped $Ga_5Ge_{20}Sb_{10}Se_{65}$ fiber following a 920 nm optical pumping; (b) pumping scheme and SWIR emission line of the Dy^{3+} ion.

Thus, despite a low pumping power, the 1.15 µm emission from the $^6H_{7/2}$ level is clearly observed in Figure 4(a). This emission shows that the $^6H_{7/2}$ level is not quenched [Figure 4(b)] and represents promising evidence that the 7.3 µm emission ($^6H_{7/2} \rightarrow {}^6H_{9/2}$ transition) can be recorded. However, the small energy gap between the $^6H_{7/2}$ and $^6H_{9/2}$ manifolds clearly indicates that the $^6H_{7/2}$ decay is dominated by multiphonon relaxation processes. A clear evidence of this non-radiative process dominance is the strong 1.4 µm emission from the $^6H_{9/2}$ manifold depicted in Figure 4(a). Under this 920 nm pumping, the $^6H_{9/2}$ level is indeed only populated through non-radiative decay from the $^6H_{7/2}$ excited state. Following this motivating result obtained in the SWIR spectral region, the LWIR luminescence properties of the 1000 ppm Dy^{3+} doped $Ga_5Ge_{20}Sb_{10}Se_{65}$ fiber were investigated and are reported in Figure 5.

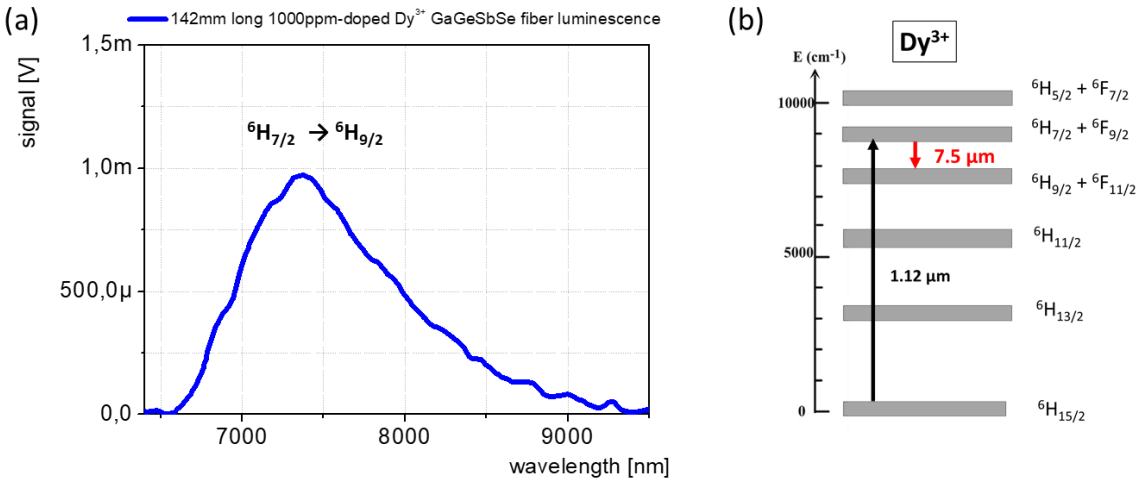

Figure 5: (a) LWIR luminescence of the Dy^{3+} ($^6H_{7/2} \rightarrow {}^6H_{9/2}$) ion in the GaGeSbSe system; (b) pumping scheme and LWIR emission line of the Dy^{3+} ion.

Figure 5(a) shows the LWIR luminescence of the Dy^{3+} doped selenide fiber spanning from 6.7 to 9 µm. The optimal fiber length for this LWIR emission depends on the propagation losses at the pump and LWIR wavelengths. Thus, after optimization of the fiber lengths, we obtained the highest LWIR emission intensity for a 142 mm long fiber, which corresponds to 93% absorption of the pump signal. The purification of this selenide fiber is assumed to limit background losses in the LWIR domain caused by the absorption from stretching vibrational modes of the Ge-O bonds. This absorption band around 7.8 µm is critical regarding the LWIR Dy^{3+} luminescence as it precisely re-absorbs the generated fluorescence [Figure 2(b)]. Therefore, the removal of Ge-O bonds from the glass structure network is strongly required to achieve a Dy^{3+} LWIR luminescence.

To further evidence the fact that this LWIR luminescence truly originates from the $^6H_{7/2}$, we recorded the intensity drop of the 1.15 ($^6H_{7/2}$), 1.4 ($^6H_{9/2}$) and 7.3 µm emission lines as a function of the pump modulation frequency. The $^6H_{7/2}$ and $^6H_{9/2}$ levels exhibit different fluorescence lifetimes (42 and 230 µs respectively in Table 2) .Thus, the $^6H_{9/2} \rightarrow {}^6H_{15/2}$ emission intensity is expected to decrease faster than the $^6H_{7/2} \rightarrow {}^6H_{15/2}$ emission intensity when increasing the pump modulation frequency [Figure 6].

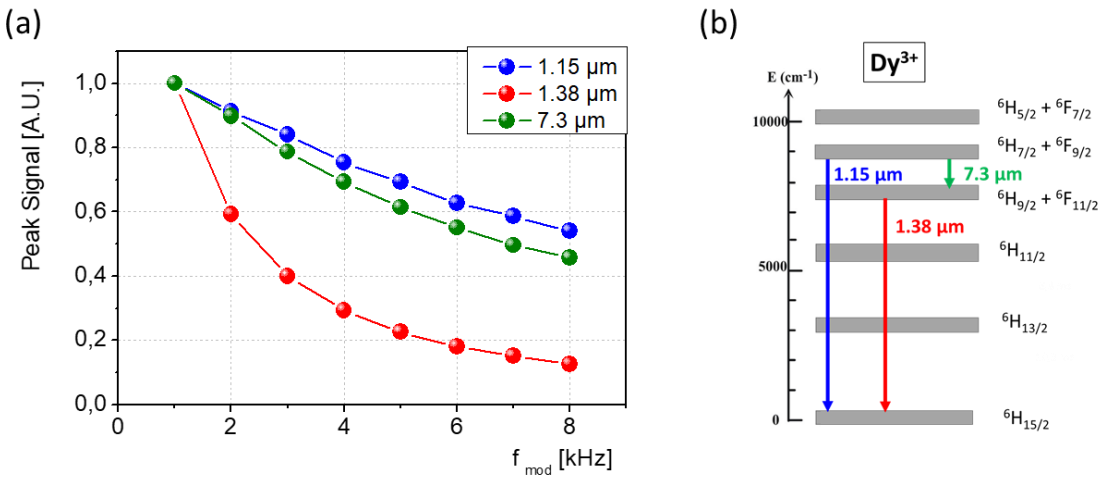

Figure 6: (a) normalized luminescence intensities of the 1.15, 1.4 and 7.3 µm emissions as a function of the pump modulation frequency; (b) Dy^{3+} level scheme showing the investigated transitions.

The 1/e fluorescence intensity drop is expected to be at 24 kHz (τ_{fluo} =42 µs, τ_{fluo}^{-1} = 24 kHz) and 4.3 kHz (τ_{fluo} =230 µs, τ_{fluo}^{-1} = 4.3 kHz) for the $^6H_{7/2}$ and $^6H_{9/2}$ levels respectively. For the $^6H_{9/2}$ manifold emission recorded at 1.4 µm ($^6H_{9/2} \rightarrow {}^6H_{15/2}$), the intensity drop in Figure 6(a) is likely faster than at 1.15µm ($^6H_{7/2}$ emission). The 1/e intensity decrease for the $^6H_{9/2}$ level expected at 4.3 kHz is in a fairly good agreement [Figure 6]. More importantly, Figure 6(a) clearly shows that the 1.15µm ($^6H_{7/2} \rightarrow {}^6H_{15/2}$) and 7.3µm ($^6H_{7/2} \rightarrow {}^6H_{9/2}$) normalized intensities present the same relative decrease, showing that these two emissions originate from the same $^6H_{7/2}$ manifold.

Finally, a raw luminescence intensity comparison of the LWIR emissions of Tb^{3+}, Sm^{3+} and Dy^{3+} embedded in the $Ga_5Ge_{20}Sb_{10}Se_{65}$ glass host was investigated and presented in Figure 7. Sm^{3+} and Tb^{3+} spectra are taken from [13], and were recorded in the same conditions with the same setup as detailed in [13].

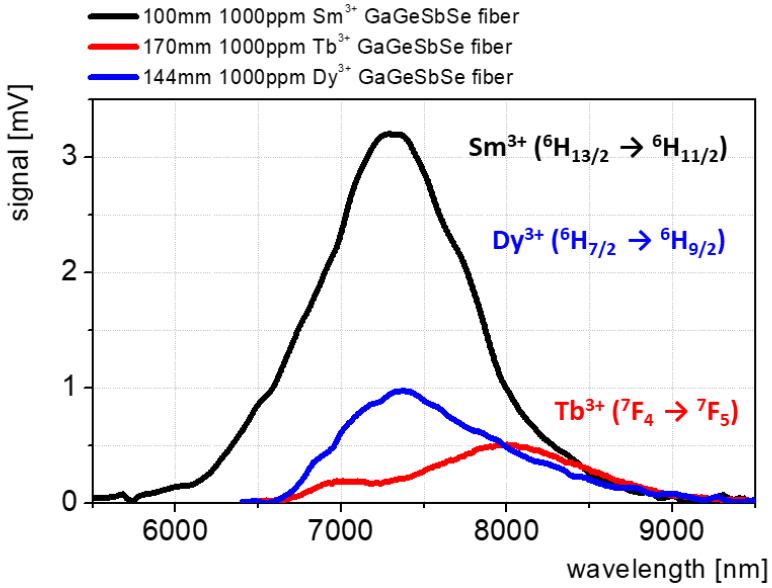

Figure 7: LWIR luminescence spectra for the Tb^{3+}, Sm^{3+} and Dy^{3+} ions in the $Ga_5Ge_{20}Sb_{10}Se_{65}$ glass host, intensities are corrected from the absorbed pump power

The Sm^{3+} and Dy^{3+} spectra emission spectra presented in Figure 7 were obtained with the same setup. The absorbed power was about 93% for the 144 mm long Dy^{3+} doped fiber and of 90% for the Sm^{3+} doped fiber. Figure 7 clearly shows that the Sm^{3+} emission is more than three times higher than the Dy^{3+} one. This is mainly due to the branching ratio difference, with a β value of 8% for the Sm^{3+} $^6H_{13/2} \rightarrow {}^6H_{11/2}$ transition and less than the percent for the Dy^{3+} $^6H_{7/2} \rightarrow {}^6H_{9/2}$ transition. Tb^{3+} and Dy^{3+} ions show comparable intensities for a similar absorbed pump power, with maximum emission wavelengths of 8.0 and 7.3 µm respectively.

4. CONCLUSION

1000 ppm Dy^{3+} doped $Ga_5Ge_{20}Sb_{10}Se_{65}$ glass preform and fibers were elaborated from conventional methods, with enhanced purification techniques. The 7.3 µm centered LWIR luminescence ($^6H_{7/2} \rightarrow {}^6H_{9/2}$ transition) from these fibers is demonstrated here for the first time to our knowledge. Alongside, a comprehensive spectroscopic study of this Dy^{3+} doped selenium based glass is presented. Absorption cross-sections and Judd-Ofelt analysis were investigated and the fluorescence lifetimes of the different emitting levels, in particular the $^6H_{7/2}$ level, were measured. Emission spectra were compared with the Dy^{3+} doped equivalent sulfide glass, illustrating the Dy^{3+} emissions phonon energy dependency in the MWIR spectral domain. The highest LWIR luminescence intensity was achieved using a 142 mm long 1000 ppm Dy^{3+} doped $Ga_5Ge_{20}Sb_{10}Se_{65}$ fiber under 1.12 µm pumping.

The authors acknowledge the support of the French Agence Nationale de la Recherche (ANR), under grant ANR-15-CE39-0007 (OPTIGAS project).

[1] S. D. Jackson, "Towards high-power mid-infrared emission from a fibre laser," *Nature Photonics*, vol. 6, p. 423, 06/28/online 2012.

[2] B. J. Eggleton, B. Luther-Davies, and K. Richardson, "Chalcogenide photonics," *Nat Photon*, vol. 5, pp. 141-148, 03//print 2011.

[3] S. Cui, C. Boussard-Plédel, J. Lucas, and B. Bureau, "Te-based glass fiber for far-infrared biochemical sensing up to 16 µm," *Optics Express*, vol. 22, pp. 21253-21262, 2014/09/08 2014.

[4] E. Baudet, Y. Ledemi, P. Larochelle, S. Morency, and Y. Messaddeq, "3D-printing of arsenic sulfide chalcogenide glasses," *Optical Materials Express*, vol. 9, pp. 2307-2317, 2019/05/01 2019.

[5] L. Bodiou, F. Starecki, J. Lemaitre, V. Nazabal, J.-L. Doualan, E. Baudet, *et al.*, "Mid-infrared guided photoluminescence from integrated Pr3+-doped selenide ridge waveguides," *Optical Materials*, vol. 75, pp. 109-115, 2018/01/01/ 2018.

[6] C. R. Petersen, U. Møller, I. Kubat, B. Zhou, S. Dupont, J. Ramsay, *et al.*, "Mid-infrared supercontinuum covering the 1.4–13.3 µm molecular fingerprint region using ultra-high NA chalcogenide step-index fibre," *Nat Photon*, vol. 8, pp. 830-834, 11//print 2014.

[7] L. B. Shaw, B. Cole, P. A. Thielen, J. S. Sanghera, and I. D. Aggarwal, "Mid-wave IR and long-wave IR laser potential of rare-earth doped chalcogenide glass fiber," *IEEE Journal of Quantum Electronics*, vol. 37, pp. 1127-1137, 2001.

[8] J. S. Sanghera, L. B. Shaw, and I. D. Aggarwal, "Chalcogenide Glass-Fiber-Based Mid-IR Sources and Applications," *IEEE Journal of Selected Topics in Quantum Electronics*, vol. 15, pp. 114-119, 2009.

[9] B. M. Walsh, H. R. Lee, and N. P. Barnes, "Mid infrared lasers for remote sensing applications," *Journal of Luminescence*, vol. 169, Part B, pp. 400-405, 1// 2016.

[10] L. Sójka, Z. Tang, D. Furniss, H. Sakr, E. Bereś-Pawlik, A. B. Seddon, *et al.*, "Numerical and experimental investigation of mid-infrared laser action in resonantly pumped Pr3+ doped chalcogenide fibre," *Optical and Quantum Electronics,* vol. 49, p. 21, 2016.

[11] N. Abdellaoui, F. Starecki, C. Boussard-Pledel, Y. Shpotyuk, J. L. Doualan, A. Braud, *et al.*, "Tb3+ doped Ga5Ge20Sb10Se65-xTex (x = 0-37.5) chalcogenide glasses and fibers for MWIR and LWIR emissions," *Optical Materials Express,* vol. 8, pp. 2887-2900, 2018/09/01 2018.

[12] F. Starecki, N. Abdellaoui, A. Braud, J.-L. Doualan, C. Boussard-Plédel, B. Bureau, *et al.*, "8 µm luminescence from a Tb3+ GaGeSbSe fiber," *Optics Letters,* vol. 43, pp. 1211-1214, 2018/03/15 2018.

[13] F. Starecki, A. Braud, N. Abdellaoui, J.-L. Doualan, C. Boussard-Plédel, B. Bureau, *et al.*, "7 to 8 µm emission from Sm3+ doped selenide fibers," *Optics Express,* vol. 26, pp. 26462-26469, 2018/10/01 2018.

[14] H. Jelínková, M. E. Doroshenko, M. Jelínek, J. Šulc, V. V. Osiko, V. V. Badikov, *et al.*, "Dysprosium-doped PbGa2S4 laser generating at 4.3µm directly pumped by 1.7µm laser diode," *Optics Letters,* vol. 38, pp. 3040-3043, 2013/08/15 2013.

[15] M. R. Majewski, R. I. Woodward, J.-Y. Carreé, S. Poulain, M. Poulain, and S. D. Jackson, "Emission beyond 4 µm and mid-infrared lasing in a dysprosium-doped indium fluoride (InF3) fiber," *Optics Letters,* vol. 43, pp. 1926-1929, 2018/04/15 2018.

[16] F. Starecki, S. Morais, R. Chahal, C. Boussard-Plédel, B. Bureau, F. Palencia, *et al.*, "IR emitting Dy3+ doped chalcogenide fibers for in situ CO2 monitoring in high pressure microsystems," *International Journal of Greenhouse Gas Control,* vol. 55, pp. 36-41, 12// 2016.

[17] F. Starecki, A. Braud, J.-L. Doualan, J. Ari, C. Boussard-Plédel, K. Michel, *et al.*, "All-optical carbon dioxide remote sensing using rare earth doped chalcogenide fibers," *Optics and Lasers in Engineering,* vol. 122, pp. 328-334, 2019/11/01/ 2019.

[18] F. Charpentier, F. Starecki, J. L. Doualan, P. Jóvári, P. Camy, J. Troles, *et al.*, "Mid-IR luminescence of Dy3+ and Pr3+ doped Ga5Ge20Sb10S(Se)65 bulk glasses and fibers," *Materials Letters,* vol. 101, pp. 21-24, 6/15/ 2013.

[19] F. Starecki, F. Charpentier, J.-L. Doualan, L. Quetel, K. Michel, R. Chahal, *et al.*, "Mid-IR optical sensor for CO2 detection based on fluorescence absorbance of Dy3+:Ga5Ge20Sb10S65 fibers," *Sensors and Actuators B: Chemical,* vol. 207, Part A, pp. 518-525, 2// 2015.

[20] V. G. Truong, B. S. Ham, A. M. Jurdyc, B. Jacquier, J. Leperson, V. Nazabal, *et al.*, "Relaxation properties of rare-earth ions in sulfide glasses: Experiment and theory," *Physical Review B,* vol. 74, p. 184103, 11/06/ 2006.

[21] W. T. Carnall, P. R. Fields, and B. G. Wybourne, "Spectral Intensities of the Trivalent Lanthanides and Actinides in Solution. I. Pr3+, Nd3+, Er3+, Tm3+, and Yb3+," *The Journal of Chemical Physics,* vol. 42, pp. 3797-3806, 1965/06/01 1965.